Observation of transient states during magnetization reversal in a quasicrystal artificial spin ice

V. Brajuskovic, A. Addi, C. Phatak, and A. K. Petford-Long

Phys. Rev. B **98**, 094424 — Published 25 September 2018

DOI: 10.1103/PhysRevB.98.094424

Observation of transient states during magnetization reversal in a quasicrystal artificial spin ice

V. Brajuskovic[1,2], A. Addi[3], C. Phatak[1,*] , A. K. Petford-Long[1,2]

[1] Materials Science Division, Argonne National Laboratory, Illinois 60439, USA
[2] Department of Materials Science and Engineering, Northwestern University, Illinois 60208, USA
[3] Department of Physics, College of DuPage, Illinois 60137, USA

Artificial spin ices (ASIs) consisting of arrays of magnetic bars are key systems in the study of geometric frustration in magnetic systems. Of particular interest are quasicrystal (QC) ASIs, in which the lack of translational symmetry and the varying coordination number of interacting bars allow for topologically-enhanced frustrated magnetization to occur. We have directly observed the formation of magnetic vortexes within the vertices of a QC ASI as a metastable transient state, during the magnetization reversal process. We observed that the vortexes primarily form in a specific subset of the vertex motif types. Micromagnetic simulations show that although these magnetic vortexes result in an increase in the local energy of the vertex before the magnetization of the bars reverses to align with the applied magnetic field, the overall energy increase is lower than the higher energy motif configurations that would result from reversal of the magnetization in the connecting bar.

I. INTRODUCTION

The study of frustrated systems is of considerable interest due to the potential of observing novel and interesting physics resulting from the residual ground-state entropy of the system.[1] Frustrated systems are those in which there is an inability to minimize the interaction energy between all pairs of components within the system. Frustration is often observed in magnetic systems, with the simplest geometry being an antiferromagnet on a triangular lattice. Frustrated magnetic systems often display interesting magnetic defect states such as magnetic monopoles defects and Dirac strings.[2] Artificial spin ices (ASIs), consisting of arrays of patterned nanoscale magnetic islands exhibit magnetic frustration when the net magnetization is unable to reach a unique ground state either due to the degeneracy of the ground state or due to the underlying lattice geometry. The first ASIs that were studied by Wang *et al.* consisted of square arrays of ferromagnetic stadia, which exhibited a "two-in-two-out" ground-state degeneracy and were observed to show a similar magnetic ordering behavior to the bulk spin ices in which the study of frustrated magnetism originated.[3] Another lattice geometry that received significant attention as interest in ASIs expanded is the hexagonal Kagome lattice. Both the square lattice and the Kagome lattice that are composed of isolated islands show magnetic monopole defects and Dirac string defects that are equivalent to those observed in bulk spin ices but with the advantage of having much more readily tunable behavior.[4] In both the square lattice and the Kagome lattice, the primary source of frustration is the geometrical frustration of the vertices which results from the inability of the ASI to minimize the interaction between all the magnetic islands that meet at a vertex.

Within the body of research on square ASIs, there has been a notable focus on methods of achieving the ground state, in addition to exploration of the various higher energy states that they can

* Corresponding Author.

adopt. In general, the most effective method for obtaining the ground state in both square and Kagome ASIs has been thermal annealing, which leads to regions (domains) in the ASI that are in a ground state separated by high energy domain walls.[5,6] Another technique commonly used to place magnetic systems into a ground state, namely demagnetization by rotating in a decreasing ac magnetic field, was found to be less effective for square ASIs than thermal annealing.[7] Studies of square and Kagome ASIs also explored the response to a magnetic field. In both *in situ* studies[8] and studies of the remnant state[9] after magnetization reversal of square lattices, it was observed that reversal occurred through the creation of pairs of magnetic monopole defects separated by a linear Dirac string that grew in linear cascades as the magnetization reversal process proceeded.

Magnetization reversal in Kagome ASIs also occurs via linear cascades.[10] Work by Farhan *et al.* explored the effects of both magnetic field and temperature by using an external magnetic field to place a Kagome ASI into a fully magnetized state and then observing how it relaxed at a temperature of 420 K.[11] In doing so, Farhan *et al.* observed that thermal relaxation differs fundamentally from athermally driven relaxation in that a strict adherence to the ice rule leads to confinement of magnetic monopole defects. Additionally, a new approach to observing ASIs in higher energy states has been described in work by Gartside *et al.*, in which they describe how topological defect-driven magnetic writing can be used to access the entire range of possible microstates in Kagome ASI.[12] There has also been interest in studying the magnetization reversal in Kagome ASIs that are composed of connected magnetic bars rather than discrete islands. In these connected ASIs, the reversal is strongly influenced by the motion of domain walls throughout the ASI, particularly in the central vertex region connecting the magnetic bars. For example, by changing the thickness of the ASI so that the domain walls change from transverse walls to vortex walls, the formation of high magnetic charge at certain vertices is suppressed. [13] Similarly, at low temperatures, domain wall pinning resulted in the magnetization reversal of connected Kagome ASIs occurring through dendritic rather than linear cascades. [14]

More recent research on ASIs has been extended to more complex lattice geometries, examples of which would be the Shakti lattice[15] and the Tetris lattice,[16] each of which is formed by removing islands from the square lattice in an ordered manner. These lattices allow for novel types of configurational frustration as a result of their geometry. Configurational frustration,[17] also known as vertex frustration, arises from the inability of every vertex in the ASI to be simultaneously in its ground state configuration. For example, in the Shakti lattice, each square plaquette has to have two high-energy vertices in order to be consistent with the neighboring plaquettes. Likewise, the ground state of the Tetris lattice decomposes into bands that are alternatingly ordered and disordered, with the disordered bands containing all the vertices that are in excited (higher energy) configurations.

All of the lattice geometries mentioned above are periodic, but recently there has also been interest in aperiodic quasicrystal (QC) ASIs, such as those in which the magnetic bars or islands are patterned on a QC lattice such as a Penrose tiling.[18] One of the distinguishing features of the QC ASIs is that the magnetic frustration in them is made more complex both by the lack of translational symmetry and by the fact that there are a relatively large number of vertex motifs with different coordination numbers and geometry. Early work on QC-ASIs focused on studying their ensemble magnetization reversal behavior and spin wave propagation upon application of a magnetic field,[19,20] in addition to the

use of micromagnetic simulations to predict their ground state configurations. More recently, the study of QC ASIs has focused on using magnetic imaging techniques to explore the ground states of both connected P2 Penrose lattices[21] and disconnected P3 Penrose lattices.[22] In the work reported in both of these papers, it was determined that the ground state of the QC ASIs could be decomposed into various sublattices, some of which demonstrated long-range order and some of which did not. Our previous work[23] on QC-ASIs patterned on a P2 Penrose tiling focused on understanding how their local and global energy changed as a function of different thermodynamic states. We had also examined the magnetization reversal of these QC-ASIs in response to an applied magnetic field and found that, unlike for periodic ASIs, the magnetization reversal proceeded via the formation of dendritic avalanches rather than via the propagation of 1D Dirac strings. However, the local changes that accompany the magnetization reversal in the bars and the effect of varying coordination on these effects has not yet been explored. Understanding this behavior can give important insights into the effects of topological frustration on magnetization reversal and lead to a better understanding of frustration in aperiodic ASIs.

In this work, we have explored in detail the energy barriers that are overcome as transient states form during the magnetization reversal process of connected QC-ASIs. The transient states are magnetic vortexes that form within the vertices at which the magnetic bars connect, prior to magnetization reversal of the surrounding bars. By observing the magnetization reversal process of the QC ASIs *in situ* during Lorentz transmission electron microscopy (LTEM) experiments, we were able to obtain quantitative, spatially-resolved information about the reversal process and the way in which the vortexes formed at a given type of vertex motif. We elucidated changes to the total energy landscape across the QC-ASI, and to the local energy variations, made possible by our ability to obtain quantitative images of the magnetic induction at individual vertices and in the surrounding bars. For example, changes to the spatial distribution and chirality of the vortexes, and to their distribution as a function of vertex motif and of vertex motif configuration (each of which has its own energy value) can be explored. By complementing our experimental observations with micromagnetic simulations of the experimental magnetic configurations that we observed, we determined how the formation of vortexes relates to the energy changes occurring during magnetization reversal within the QC ASI. This is despite the fact that vertices containing a vortex have a higher energy than the equivalent vertex motif configuration without a vortex, even accounting for the energy contributed by the applied field.

II. EXPERIMENT

We fabricated QC ASIs based on a 3rd generation P2 Penrose tiling: 20 nm thick films of Permalloy (Py) were sputter deposited onto a 50 nm thick Si_3N_4 membrane window supported by a Si TEM chip. The Py thin film was then patterned to form a QC ASI using direct focused ion-beam milling. The resulting structure is shown in Figure 1a. The P2 Penrose tiling is formed from 'darts' and kites' and the tiling contains two different bar lengths: the long bars have a length of 2.03 μm and the short bars have a length of 1.3 μm, with all bars having a width of 200 nm. A number of QC-ASI P2 tilings were patterned, in orientations such that the in-situ applied field would run either parallel to one of the high-symmetry directions (orange dashed line in Fig. 1a) or to one of the low-symmetry directions (white

dashed line in Fig. 1a), so that the effects of geometrical orientation on the magnetization reversal process could be determined. There is an angle of 18° between the two directions.

The spatially-resolved magnetic configuration across the QC-ASIs was determined from Fresnel-mode Lorentz TEM images, using an aberration-corrected dedicated magnetic imaging instrument in which the sample sits in a very low vertical field (< 10 G).[24] In order to easily observe the Fresnel contrast arising from the magnetization configuration in the bars and at the vertices, a large defocus value of Δf = −27 mm was used. The response to an in-plane applied magnetic field was recorded using an *in-situ* magnetizing holder. Fresnel images of each of the QC ASI lattices were recorded at various values of applied field as it was swept from +800 G to −800 G, in order to fully saturate the sample in both directions. However, an image of the sample can only be seen for values between approximately ±200 G because of the limited beam tilt in the microscope, and so all data presented will be in the −200 G to +200 G range.

In order to extract quantitative information about the energy landscape across the QC-ASI, we carried out micromagnetic simulations using the OOMMF software.[25] The simulation parameters used were: exchange constant, $A = 1.3 \times 10^{-11}$ J ·m^{-1}; anisotropy constant, $K = 0$; saturation magnetization, $M_S = 8.6 \times 10^5$ Am^{-1}. The different vertex motifs were simulated individually, and the total size of each simulation was 4.5 µm × 4.5 µm × 20 nm, with a cell size of 5 nm × 5 nm × 5 nm. The initial magnetization configuration of the vertex motif was input from a bitmap, and we used an Euler evolver to relax the simulation. Vortexes were simulated by setting the initial magnetization in the central region of a vertex motif to be either a clockwise or counterclockwise vortex with the initial magnetization in the surrounding bars set to be single domain (as is observed experimentally). The simulation was allowed to relax for 100 steps so as to smooth the boundaries between the different regions, but a full relaxation was not done so that the higher energy vortex state would not be relaxed out.

III. RESULTS

As discussed above, we explored the behavior of Penrose P2-tiled QC ASIs with a high-symmetry or low-symmetry direction parallel to the applied field, so that the effects of geometrical orientation on the magnetization reversal process could be determined. Figure 1a shows an out-of-focus bright-field TEM image of the QC ASI for which the field is applied along a low symmetry direction (i.e. parallel to the white dashed line). The orange dashed line indicates one of the five equivalent high symmetry directions. The pale contrast region surrounding the magnetic bars is the SiN support membrane. Figure 1b shows an enlarged image of one of the Py bars: the magnetization direction in each of the bars was determined from the gradient of intensity across the bar: the red arrow indicates the direction of the gradient from light to dark, and the green arrow indicates the corresponding direction of magnetization. Figure 1c shows a line plot of the grayscale intensity in the image across the position of the blue line indicated in Figure 1b. The red arrow in Figure 1c corresponds to the direction of the gradient as shown in Figure 1b.

The magnetization directions in the bars were determined for each value of the *in-situ* applied field, enabling the component of net magnetization for the entire lattice to be determined. From these values, hysteresis loops of the component of magnetization parallel to the applied field could be

calculated as a function of applied field, as shown in Fig. 1d. The blue triangles correspond to the QC-ASI for which the field is applied along a high-symmetry direction, and the green circles correspond to the field being applied along a low-symmetry direction (a rotation of 18° relative to the high-symmetry direction). The black arrows next to each branch of the hysteresis loops indicate the direction of the field sweep. It should be noted that the hysteresis loops shown in Figure 1d are offset to the left by 25 G, which results from the 25 G residual field in our *in situ* magnetizing holder. Taking this into account, the coercivity for the field applied along a high-symmetry axis is 50 G, and the coercivity for the field applied along a low-symmetry axis is 100 G. This suggests that the high-symmetry direction is an easier axis for magnetization reversal. As for our previous studies, the magnetization reversal in all of the QC ASIs proceeds via dendritic cascades of bars reversing their magnetization direction. However, for the high-symmetry axis reversal (blue curve in Fig. 1d), the first bars to reverse were predominantly those with magnetization aligned exactly antiparallel to the applied field direction, which act as initiation sites for the dendritic cascades. Their reversal can be seen from the large jumps (seen at approximately −25 Oe and +25 Oe) in the blue hysteresis curve. In contrast, for reversal along the low symmetry direction (green curve in Fig. 1d), for which there are no bars with magnetization lying exactly antiparallel to the applied field, there are no large jumps in the hysteresis loop. This corresponds to the fact that there are no clusters of bars that reverse their magnetization collectively in response to the applied field.

Each of the QC-ASIs is composed of six different vertex motifs in the interior of the lattice, in addition to three different 'truncated' edge motifs with lower symmetry. As a result of the truncated nature of the edge motifs, we have chosen only to focus on the interior vertex motifs, for which micromagnetic simulations are shown in Figure 2a. The direction of magnetization in each of the bars corresponds to the color wheel to the right, and in each case the motif is shown with the magnetization in the lowest energy configuration. Vertex motifs 1 and 2 have coordination numbers of 3 and 4, respectively. This results in those motifs having fewer low energy states when compared with motifs 3–6, all of which have a coordination number of 5. During the magnetization reversal process, the appearance of a vortex configuration was seen for a number of the vertices, as a transient configuration prior to magnetization reversal of the surrounding bars. Figs. 2b and 2c show Fresnel mode out-of-focus LTEM images of two different Motif-2 vertices, each with a vortex that formed in the vertex. Counterclockwise vortexes appear as white dots (Fig. 2b) and clockwise vortexes appear as black dots (Fig. 2c). Motif-2 vertices accounted for the largest number of vortexes that formed, although some vortexes were observed for all of the motifs.

Micromagnetic simulations of the motifs both with, and without, a vortex were performed for each value of the field at which the vortexes were observed, and for each of the possible magnetization configurations of the motifs. Fig. 2d shows one such micromagnetic simulation for a Motif-2 vertex with a counterclockwise vortex. The micromagnetic simulations enabled us to determine the energy of each vertex motif for each of its different magnetization configurations, and these are plotted in Figure 3. The number on the *x*-axis indicates the vertex motif number, and the energies of the configurations (in J) are shown by the grey dots directly above each number. To the right of each motif number are shown the energies of one or more specific magnetization configurations either with a vortex (orange dot) or without a vortex (grey dot). The vertical gap between the grey and orange dots indicates the energy of

formation of the vortex. For cases where two orange dots with a different energy have grey dots with the same energy underneath, the difference between the two orange dot energies is a result of the vortex chirality direction. From Figure 2e, we see that the energy required to form a vortex is approximately of the same order as the energy required to put a vertex into a higher energy magnetic configuration, but is considerably lower than placing any of the vertex motifs into their highest energy configuration.

Each time the applied field was swept around the hysteresis loop, we recorded the appearance of each of the vortexes, including vertex motif type, motif magnetization configuration and applied field value at which it appeared. We focused only on vortexes that appeared prior to reversal of the magnetization in the adjacent bars. The number of vertices for each motif in which a vortex formed are summarized in Figure 4 for a sweep from positive to negative field, which corresponds to the left-hand side of the blue and green curves in Fig. 1d. Fig. 3a shows data for the field applied along a low-symmetry direction of the QC-ASI, and Fig. 3b shows data for a field applied along a high-symmetry direction. The trends observed for both applied field orientations were very similar to those seen for the field sweep from negative to positive. The total height of each bar shows the total number of vortexes that appeared at the corresponding field value, and the different colors relate to the different motifs as indicated in the legend. For the field applied along a low-symmetry direction (Fig. 3a) the vortexes appear primarily in motifs 1, 2, and 5, with vortexes tending to form first in Motif-5 vertices (cyan), then in Motif-2 vertices (red), and finally in Motif-1 vertices (blue). The orange bars show the appearance of a few vortexes in Motif-6 vertices. For the field applied along a high-symmetry direction (Fig. 3b) vortexes form in all the vertex-motif types, appearing first for Motif-2 vertices (red), followed by a few vortexes in vertices of motif-type 3 (green), 4 (purple), 5 (cyan) and 6 (orange). The final vortexes to form appear in Motif-1 vertices (blue). Overall, in comparison with the low-symmetry field direction, more vortexes form for the field applied along the high-symmetry field direction (54 versus 33), and in a wider range of vertex motifs, with the Motif-5 vortexes preceded by the Motif-2 vortexes. Additionally, the vortexes form over a wider field range. Figure 3c shows the percentage of vertices that form a vortex for each motif, for the field applied along the low-symmetry (grey bars) and high-symmetry (orange bars) directions. The data for Fig. 3c were obtained by combining the results for a single up and down sweep for two different QC ASIs, for the field applied along the low-symmetry direction and by combining the results for a single up and down sweep for one QC ASI for the field applied along the high symmetry direction. Note that the number of vertices of each motif type in our QC-ASIs varies considerably: five for motif 6, six for motif 3, ten each for motifs 4 and 5, twenty-five for motif 2 and thirty-five for motif 1.

We further examined whether there was a relationship between the vortex nucleation field and the location of the corresponding motif within the QC-ASI. Figure 4 shows schematics of the spatial distribution of the vortexes that form, as a function of applied field swept from positive to negative values. The data shown in Figure 4 are for single field sweeps, and are representative of what was observed over a number of field sweeps carried out during our experiments. It should be noted that the process by which the vortexes form is stochastic, such that repeated field sweeps do not necessarily result in the vortexes forming at the exact same vertices at the exact same field. Additionally, on very

rare occasions during the field sweeps that we observed, more than one vortex formed within a single vertex at different field values. However, the general trends across the six vertex motifs, in terms of the order in which they form vortexes, and the number of vortexes that form, *are* repeatable, and so we have focused on these general trends in this paper. The large black arrow shows the direction of the positive applied field. The colored dots show the location of the vortexes and the dot color indicates the field value at which the vortex appeared (see legend to right of Fig. 4). In several of the Motif-5 vertices two vortexes formed during the magnetization reversal process at different field values, as shown by pairs of dots. The small black arrows within the bars surrounding each vertex containing a colored dot show the magnetization configuration in the vertex motif at vortex nucleation field. For the circled bars in Fig. 4b, the direction of magnetization reversed between the formation of vortexes in the adjacent vertices: the color of the arrowhead indicates the direction of magnetization at the applied field at which the similar colored vortex appeared. For all the vortexes that were observed, there is no clear relationship between the vortex nucleation field value and their location within the ASI.

Vortexes formed most often in the Motif-2 vertices, and so we studied these motifs in more detail. Schematics showing the correlation between vortex chirality (clockwise or counterclockwise) within the Motif-2 vertices, and the motif orientation with respect to the applied field, are seen in Figure 5. The values indicate the angle between the y-axis of the Motif-2 vertex (inset) and the applied field direction (green arrow). Fig. 5a shows summed data for two QC-ASIs with field applied along the low-symmetry direction, and Fig. 5b shows data for a QC-ASI with field applied along the high-symmetry direction. The red dots correspond to vortexes with counterclockwise chirality, and the blue dots indicate vortexes with clockwise chirality. For the low symmetry field direction there is clear clustering of the vortex chirality: for Type-2 motifs with *y*-axis making an angle of 0°–180° with respect to the field direction, the vortexes have counterclockwise chirality. For those making an angle between 180°–360° the vortexes have clockwise chirality. For the field applied along a high-symmetry direction the overall trend is similar, although the split between the two chiralities is not along the field direction, a similar division occurs except in this case Motif-2 vertices whose angle with the applied field is 54°-234° tend to form counterclockwise vortexes with the rest tending to form counterclockwise vortexes. Nevertheless, Fig. 5 shows that there exists a correlation between vortex chirality and motif orientation. A similar trend is also seen for the other vertex motifs, but the low number of vortexes observed in those motifs means that we have not included these data here.

IV. DISCUSSION

In this work, we are primarily concerned with the configurational frustration of the entire QC-ASI, namely the inability of all of the vertices to be simultaneously in a ground state configuration, and how the different vertex motifs contribute to controlling the energy landscape. The ground-state energy configuration of the Motif-3 vertices is highly degenerate as a result of the five-fold rotational symmetry. As a result, the Motif-3 vertices are likely to remain in their lowest energy configuration when bars reverse their magnetization direction. Vertex motifs 4, 5 and 6 only show mirror symmetry, however as shown in our previous work,[23] the energy spectra for these motifs contain a cluster of closely-spaced energy levels towards the bottom. As a result, the energy cost of a bar reversing its magnetization direction in one of these vertex motifs is often trivial. Motif-1 and Motif-2 vertices, on the

other hand, have fewer, more distinct energy states, with energy values that are more widely separated. As a result, the magnetization reversal of a bar in a Motif-1 or a Motif-2 vertex is likely to put it in a higher energy configuration. As a result, the average energy penalty for having a single bar reverse in vertices with higher coordination number (motifs 3 to 6) is lower than that for those with lower coordination number (motifs 1 and 2). Thus, vertex motifs 3 through 6 are more likely to stay in their lower energy configurations even after the magnetization in the motif bars reverses while vertex motifs 1 and 2 are more likely to be put into a higher energy configuration by having the magnetization in a bar reverse.

This is indeed what we see experimentally and from simulations. This is in contrast to changes in the magnetization configuration for the Type-1 and Type-2 vertices, which have a lower coordination number, which often place these vertex motifs into higher energy configurations. Since the bars are connected, magnetization reversal of a bar associated with one vertex automatically also affects the configuration (and thus the energy) of the adjacent vertex, which means that during the magnetization reversal process, Motif-1 and Motif-2 vertices are most likely to be forced into their highest energy configuration to retain lower-energy configurations for the adjacent 5-bar motifs. Indeed, if we consider pairs of vertices for which a vortex nucleates in one of the vertices, we observe that if magnetization reversal of the common bar occurred, the combined energy increase of resultant configurations of the two vertices would have much higher energy (and magnetic frustration) than that imparted to the ASI by formation of the vortex. Furthermore, we believe that the vortexes are not an important factor in achieving the ground state. In our previous work on QC-ASIs[23], we found that demagnetizing in a rotating magnetic field achieved the state that most closely approached the ground state. Since we observed no vortexes to form within the rotationally demagnetized state, it is more likely that the vortexes are instead associated with higher energy states. The vortex nucleation can therefore be seen as an intermediate (transient) state that allows the energy of the QC-ASI to evolve without the requirement for a change in magnetization configuration of a pair of vertices and thus a large increase in the overall energy of the ASI. As can be seen from Fig. 4, the vortices form most often at vertices connected to an adjacent Motif-1 vertex that would be forced into its *highest* energy configuration by the magnetization reversal of the common bar, as illustrated schematically in Figure 6. Fig. 6a shows connected Motif-1 and Motif-5 vertices before magnetization reversal occurs, with the black arrows indicating the direction of magnetization in each bar. Fig. 6b shows the change in magnetic configuration that would occur if magnetization in the connecting bar, indicated with a red arrow, reverses. The blue arrow indicated the applied magnetic field. Both the Motif-1 and Motif-5 vertices are put into high energy configurations, as indicated by the red circles. When this reversal occurs, usually along with the reversal of several of its neighbors as part of a dendritic cascade, the vortex disappears.

All vertex motifs are capable of supporting vortexes, but it is primarily vertex motifs with lower coordination number such as the Motif-1 and Motif-2 vertices that accommodate the excess energy put into the ASI by nucleating vortexes. As in our previous work, this suggests that Motif-1 and Motif-2 vertices are sites of high frustration within the QC ASI. However, it is notable that motif-5 vertices also show a more regular tendency to form vortexes than Motif-3, -4, and -6 vertices despite the fact that all of these vertex motifs have multiple lower energy configurations and all contain five bars. One way in

which the Motif-1, -2, and -5 vertices are similar to each other, and are different from the Motif-3, -4, and -6 vertices, is that their lowest energy states, as illustrated in Fig. 2, contain a domain wall within the central vertex region. As the reversal process occurs, these vertex domain walls can evolve relatively easily into magnetic vortices. Now, considering only the Motif-1, -2, and -5 vertices, the reason that vortices tend to nucleate in the Motif-5 vertices earlier on in the reversal is that their central vertex region is the largest, which allows for more stable vortexes to form. The central vertex region of Motif-2 vertices is the second largest, with Motif-1 vertices having the smallest central vertex region. This is consistent with the trends observed in Fig. 3 in terms of the order in which vortexes form, for the low-symmetry field direction. For the high-symmetry field direction, the percentage of Motif-3 and Motif-6 vertices in which a vortex forms increased substantially. We believe that this occurs because applying a field along the high symmetry direction increases the likelihood that Motif-3 and Motif-6 vertices meet the condition described in Fig. 6, although the stochastic nature of the vortex formation and the small number of Motif-3 and Motif-6 vertices means that there is likely considerable statistical deviation. We believe that Motif-1, Motif-2, and Motif-5 vertices are still most significant in terms of vortex formation as they consistently showed vortex formation across all experiments.

The fact that the vortexes formed quite isotropically throughout the QC ASIs suggests that there is no positional dependence affecting vortex formation. This, in turn, suggests that the magnetic interactions that lead to vortex formation are primarily short range, as might be expected from the bar length. In general, because the vortexes appeared before magnetization reversal in surrounding bars occurred, we found that vortexes primarily appeared in vertices whose magnetization configuration was consistent with having a fully aligned QC ASI and in which the bar magnetizations were close to antiparallel to the applied field. These configurations tend to be among those with lower energy for each vertex motif. The observation (shown in Fig. 5b) that the split between vortexes with clockwise or counterclockwise chirality occurred along a line at 36° to the applied field, for the high-symmetry field direction, was unexpected as the split would be expected along the applied field direction. However, it should be noted that the direction of the split is also a high-symmetry direction, and thus it is possible that the observation is a result of stochastic deviation from the expected value. Vortexes form due to energetic considerations for a pair of neighboring vertices rather than a single vertex. As a result, it could be that the relative orientation of a vertex in addition to one of its neighbors is what determines the sense of the vortex that results. Additionally, because the magnetization in the QC ASI is aligned before reversal occurs, the orientation of the Motif-2 vertex relative to the applied field is related to its configuration. As was seen in Fig. 2e, there is an energy difference between clockwise and counterclockwise vortexes for the same configuration. It could be this energy difference that results in the preferential formation of a clockwise or counterclockwise vortex for a given orientation of a Motif-2 vertex relative to the direction of the applied field.

V. CONCLUSION

In summary, we have carried out quantitative analysis of the formation of metastable vortex transition states in QC-ASIs during magnetization reversal. The ability to image these ASIs *in situ* during the reversal process, with high spatial resolution, allows us to focus on the local magnetization behavior in the QC-ASIs. Although such metastable states can be “frozen in” and then observed using *ex situ*

techniques, the ability to observe when and where they form is of vital importance to understanding their formation. By Observing the vortexes nucleating at vertices prior to magnetization reversal of the surrounding bars, and their subsequent disappearance when the bar magnetization reversed, we determined that they are associated with the overall magnetization reversal of the QC-ASI. Our quantitative imaging technique also allows for the creation of more accurate initial configurations for micromagnetic simulations. In turn, this enabled us to obtain values for the energy of formation of the vortexes. These observations allow us to develop more insight into the propagation of solitons and domain walls in connected QC ASIs.

We have shown that vortexes form in the vertices of a connected QC-ASI during the magnetization reversal process. The vortexes are a transient state that accommodates the energy added to the QC ASI by the external applied magnetic field, as a vortex state was often lower in energy than the resulting configurations from reversing the magnetization in certain bars. While all of the vertex motifs exhibited the formation of vortexes, we were able to conclude that the relative dearth of lower energy configurations available to Motif-1 and Motif-2 vertices, relative to the Motif-3 through Motif-6 vertices, resulted in those vertices being sites of high frustration during magnetization reversal in QC ASIs. Finally, we were able to observe that the relative orientation of each of the vertex motifs to the direction of the applied field correlated to the sense of the vortex that was observed to form.

ACKNOWLEDGEMENTS

This work was supported by the US Department of Energy, Office of Science, Office of Basic Energy Sciences, Materials Science and Engineering Division. Use of the Center for Nanoscale Materials was supported by the US Department of Energy, Office of Science, Office of Basic Energy Sciences, under contract no. DE-AC02-06CH11357. We acknowledge J. Pearson for help with thin film deposition. A. Addi thanks the National Science Foundation for support for a summer intern position at Argonne under grant DUE-1564720 “Promoting STEM Student Success through Individualized Coaching and Interdisciplinary Community.”

[1] K. Matsuhira, Y. Hinatsu, and T. Sakakibara, *J Phys.: Condens. Matter.* **13,** L737 (2001).
[2] C. Castelnovo, R. Moessner, and S. L. Sondhi, *Nature* **451**, 42 (2008).
[3] R. F. Wang, C. Nisoli, R. S. Freitas, J. Li, W. McConville, B. J. Cooley, M. S. Lund, N. Samarth, C. Leighton, V. H. Crespi, and P. Schiffer, *Nature* **439**, 303 (2006).
[4] L.J. Heyderman and R.L. Stamps, *J. Phys.: Condens. Matter* **25**, 363201 (2013).
[5] S. Zhang, I. Gilbert, C. Nisoli, G.W. Chern, M. J. Erickson, L. O’Brien, C. Leighton, P. E. Lammert, V. H. Crespi, and P. Schiffer, *Nature* **500**, 553 (2013)
[6] J. P. Morgan, A. Stein, S. Langridge, and C. H. Marrows, *Nat. Phys.* **7**, 75 (2011).
[7] J. P. Morgan, J. Akerman, A. Stein, C. Phatak, R. M. L. Evans, S. Langridge, and C. H. Marrows, *Phys. Rev. B* **87**, 024405 (2013)

[8] C. Phatak, M. Pan, A. K. Petford-Long, S. Hong, and M. De Graef, *N. J. Phys.***14**, 075028 (2012).
[9] J. P. Morgan, A. Stein, S. Langridge, and C. H. Marrows, *N. J. Phys*. **13**, 105002 (2011).
[10] E. Mengotti, L. J. Heyderman, A. F. Rodríguez, F. Nolting, R. V. Hügli, and H. B. Braun, *Nat. Phys.* **7**, 68 (2011).
[11] A. Farhan, P. M. Derlet, L. Anghinolfi, A. Kleibert, and L. J. Heyderman, *Phys. Rev. B* **96**, 064409 (2017).
[12] J. C. Gartside, D. M. Arroo, D. M. Burn, V. L. Bemmer, A. Moskalenko, L. F. Cohen, and W. R. Branford, *Nat. Nano.* **13**, 53 (2018).
[13] S. Ladak, S. K. Walton, K. Zeissler, T. Tyliszczak, D. E. Read, W. R. Branford, and L. F. Cohen,*New J. Phys.* **14**, 045010 (2012).
[14] K. Zeissler, M. Chadha, E. Lovell, L. F. Cohen, and W. R. Branford, *Sci. Rep.* ***6,*** 30218 (2016).
[15] M. J. Morrison, T. R. Nelson, and C. Nisoli, *New J. Phys.* **15**, 045009 (2013).
[16] I. Gilbert, Y. Lao, I. Carrasquillo, L. O'Brien, J. D. Watts, M. Manno, C. Leighton, A. Scholl, C. Nisoli, and P. Schiffer, *Nat. Phys.* **12**, 162 (2016).
[17] C. Nisoli, V. Kapaklis, and P. Schiffer, *Nat. Phys.* **13**, 200 (2017).
[18] V. S. Bhat, J. Sklenar, B. Farmer, J. Woods, J. T. Hastings, S. J. Lee, J. B. Ketterson, and L. E. De Long, *PRL* **111**, 077201 (2013).
[19] B. Farmer, V. S. Bhat, J. Sklenar, J. Woods, E. Teipel, N. Smith, J. P. Ketterson, J. T. Hastings, and L. E. De Long, *J. App. Phys.* **115**, 17E133 (2014).
[20] V. S. Bhat, J. Sklenar, B. Farmer, J. Woods, J. B. Ketterson, J. T. Hastings, and L. E. De Long, *J. App. Phys.* **115**, 17C502 (2014).
[21] B. Farmer, V. S. Bhat, A. Balk, E. Teipel, N. Smith, J. Unguris, D. J. Keavney, J. T. Hastings, and L. E. DeLong, *Phys. Rev. B* **93**, 134428 (2016).
[22] D. Shi, Z. Budrikis, A. Stein, S. A. Morley, P. D. Olmsted, G. Burnell, and C. H. Marrows *Nat. Phys.* **14**, 309 (2018).
[23] V. Brajuskovic, F. Barrows, C. Phatak, and A. K. Petford-Long, *Sci. Rep.* **6**, 34384 (2016).
[24] M. De Graef and A. K. Petford-Long, in *Characterization of Materials*, edited by E.N. Kaufmann (John Wiley and Sons, Hoboken NJ, 2012) 1787.
[25] M. J. Donahue and D. G. Porter, OOMMF User's Guide, Version 1.0, 1999

Figures:

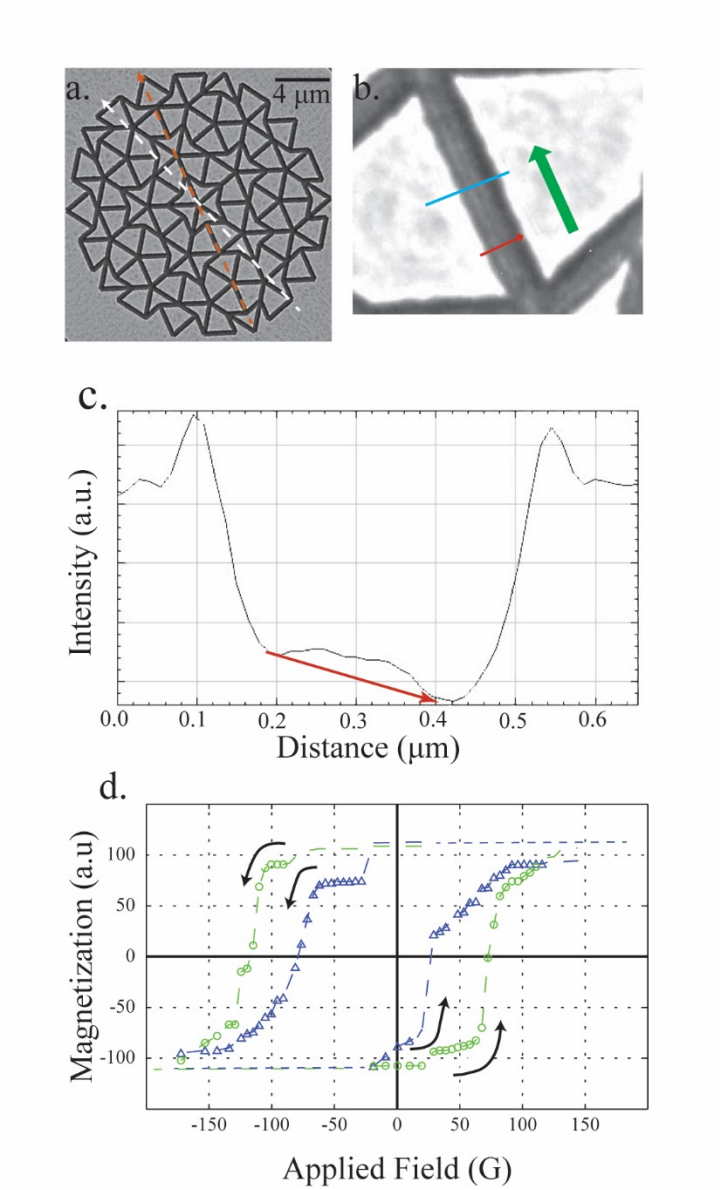

Figure 1—See online for color. a) A bright field TEM image of a QC ASI. The orange dashed line indicates a direction of high symmetry along the QC ASI and the white dashed line indicates a direction of low symmetry along the QC ASI. b) A closeup view of one of the bars in the QC ASI. The green arrow indicates the direction of magnetization as determined by the direction of the intensity gradient represented by the red arrow. c) A graph showing the intensity as a function of distance along the blue line in b). d) Hysteresis loops for magnetization reversal with the applied field along the high symmetry direction shown with blue triangles and along the low symmetry direction shown with green circles. The black arrows next to each branch of the hysteresis loops indicate the direction of the field sweep.

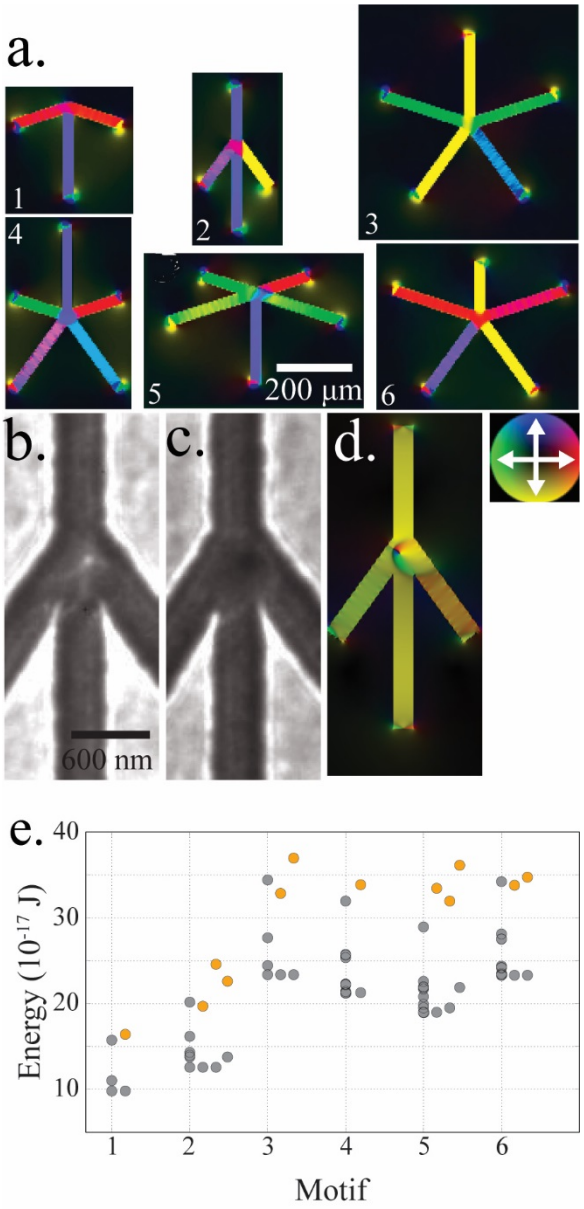

Figure 2—See online for color. a) Micromagnetic simulations for vertex motifs 1–6 in their lowest energy configuration. The color in each bar shows the direction of magnetization as indicated by the color wheel on the right. b) Fresnel contrast LTEM image of a counterclockwise magnetic vortex in a Motif-2 vertex, which appears as a white dot. c) Fresnel contrast LTEM image showing a clockwise magnetic vortex (black dot). d) Micromagnetic simulation of a clockwise vortex as seen in c). e) Plot showing the energy calculated from micromagnetic simulations for having a vortex in each of the vertex motifs. The orange dots indicate the energy of a motif configuration with a vortex in it and the gray dots underneath indicate the energy of the corresponding configuration with no vortex. For two orange dots corresponding to a gray dot with the same energy value, the difference represents the difference in energy between a clockwise and counterclockwise vortex. The gray dots to the left for each vertex motif show the energies of all the configurations without a vortex. Only the configurations in which vortexes were observed experimentally were simulated.

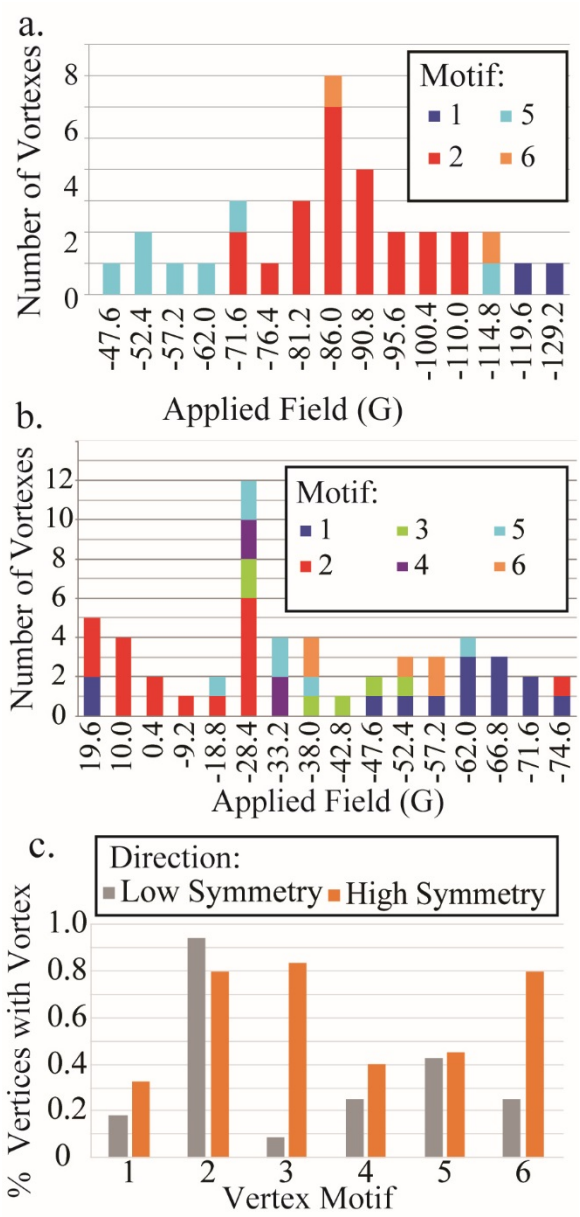

Figure 3—See online for color. a) A graph showing the number of vortexes that formed as a function of applied field, for the field applied along a low symmetry direction. Each bar is divided into one or more colors indicating the number of vortexes that formed in each motif type (see key below). b) A graph showing the same information as in a) but with the applied field along a high-symmetry direction. c) A graph showing the percentage of each vertex motif in which a vortex was observed, for the low-symmetry field direction (gray) and the high-symmetry field direction (orange).

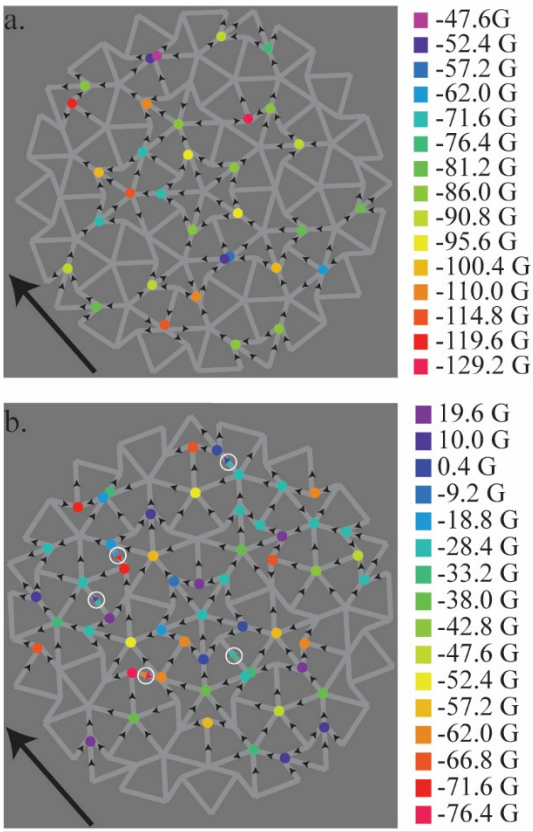

Figure 4— See online for color. a) Schematic of a QC-ASI with dots showing the location at which a magnetic vortex formed, for field applied along a low-symmetry direction. The dot color indicates the applied field value at which the vortex formed (see key to the right). The small black arrows indicate the direction of magnetization in the bars surrounding each vortex at the vortex-formation field. For those bars with a two-colored double-headed arrow, the arrow color indicates the magnetization direction of magnetization in the bar at the field at which the vortex indicated by the similarly-colored dot formed. The large black arrow indicates the positive direction of applied field. b) The same schematic as a) but for the applied field along a high-symmetry direction.

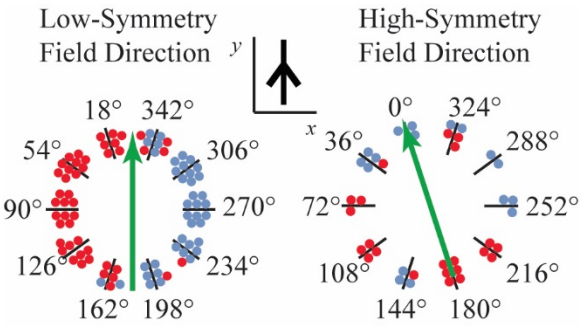

Figure 5— See online for color. A schematic showing the sense of the vortexes that were observed in Motif-2 vertices as a function of the orientation of each motif-2 vertex relative to the applied field direction (indicated by the green arrow). The angle corresponds to that of the y-axis of the motif-2 vertex, shown in the inset, compared to the applied field direction. A red dot indicates a counterclockwise vortex and a blue dot indicates a clockwise vortex. Data are shown for the applied field along both the low-symmetry and high-symmetry directions.

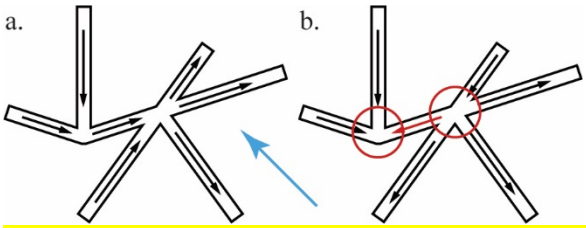

Figure 6—See online for color. a) A schematic showing the configurations of connected Motif-1 and Motif-5 vertices before any magnetization reversal. The black arrows indicate the direction of magnetization in the bars. b) After a field is applied along the direction indicated by the blue arrow, the magnetization in the connecting bar reverses (red arrow). This results in high-energy configurations for both the motif-1 vertex (three bars pointing in) and the motif-5 vertex (four bars pointing out) (red circles).